Thermodynamic μT model of ultrafast magnetization dynamics

B. Y. Mueller* and B. Rethfeld

Department of Physics and Research Center OPTIMAS, University of Kaiserslautern, Erwin-Schrödinger-Strasse 46, 67663, Kaiserslautern, Germany

(Received 7 April 2014; revised manuscript received 26 June 2014; published 16 October 2014)

Exciting a ferromagnetic sample with an ultrashort laser pulse leads to a quenching of the magnetization on a subpicosecond time scale. On the basis of the equilibration of intensive thermodynamic variables, we establish a powerful model to describe the demagnetization process. We demonstrate that the magnetization dynamics is mainly driven by the equilibration of chemical potentials. The minimum of magnetization is revealed as a transient electron equilibrium state. Our method identifies the slowing down of ultrafast magnetization dynamics by a critical region within a magnetic phase diagram.

DOI: 10.1103/PhysRevB.90.144420 PACS number(s): 75.78.Jp, 05.70.Ln

I. INTRODUCTION

The strong increase of computational power within the last 30 years has also boosted the need for large and fast data storage. However, the physical speed limits of conventional magnetic recording, which are on the order of nanoseconds, are nowadays reached [1]. A promising enhancement lies in a subpicosecond change of magnetization, as was found in 1996 by exciting a ferromagnetic material with an ultrashort laser pulse [2]. However, a detailed understanding of the underlying physical processes of this ultrafast demagnetization is still lacking and several models compete, hampering further development [3–6].

The most promising concepts are based on superdiffusive spin transport [7–10] or Elliott-Yafet (EY) spin-flip processes [5,6,11–21]. It has been shown experimentally that both processes contribute to the magnetization dynamics, depending on the sample geometry [3,9]. On the one hand, superdiffusive transport dominates on bulk and multilayer systems and has been successfully compared to experiments [8,9]. On the other hand, EY spin-flip scattering has been investigated with kinetic models and reproduces the magnetization dynamics for thin films [14–16]. Due to the complexity of these methods, temperature-based models have been proposed, like the microscopic three temperature model (M3TM) [12,21]. Recently, it has been shown, that this simplification is justified, despite an ultrafast laser excitation [14].

In this paper, we derive a μT model (μTM), which traces the dynamics and the equilibration of temperatures (T) and chemical potentials (μ) of the electron subsystems simultaneously. The essential concepts of the μTM are based on a kinetic approach [13–15], including EY-type spin-flip scattering and a dynamic exchange splitting [11,14]. The μTM reproduces the experimental magnetization curves for different laser fluences. We find that the equilibration of chemical potentials drives the dynamics of the magnetization and the magnetization minimum is revealed as a transient equilibrium state in a magnetic phase diagram. We identify a critical region within this phase diagram: For certain fluences, the material is driven into this region, causing an extreme deceleration of the magnetization dynamics. This finding confirms the experimental observation of a critical slowing down [12,21]. Unlike the M3TM, we trace the dynamics of minority and majority electron densities explicitly, which opens the possibility to extend the model for superdiffusive transport effects.

II. THEORY

A general matrix formulation of a time- and space-dependent coupled transport equation [22] is given by

$$C\frac{d}{dt}\vec{X} = \nabla K \nabla \vec{X} + G\vec{X} + \vec{S}, \tag{1}$$

where $\vec{X}$ is the vector of transient variables; C, K, and G are matrices of capacities, transport, and coupling, respectively; and $\vec{S}$ is the source vector. A representative of such an equation is the well known two-temperature model (TTM) [23] of two coupled heat conduction equations. In that case, the vector of interest $\vec{X}$ consists of the respective electron and lattice temperature T_e and T_ℓ, the source vector contributes to the equation for the electron energy, and the capacity matrix as well as the transport matrix are diagonal matrices. The temperatures are coupled through an equilibration term $\pm g(T_e - T_\ell)$, thus the coupling matrix G contains also off-diagonal elements, where g denotes the electron-lattice coupling parameter.

For ferromagnetic materials, usually two completely different approaches are applied. First, the Heisenberg model for localized magnetic moments which introduces magnons and second the Hubbard model which leads to the Stoner model within a mean field approach [24]. We presume that both the Heisenberg model and Hubbard model are applicable to ultrafast magnetization dynamics [14,25] and the truth lies between both models [26]. Recent *ab initio* calculations showed that electron-magnon interaction alone might not explain the demagnetization on an ultrashort time scale [27], however, magnons can be created by the decay of Stoner excitations for longer times [28,29]. In this work, we apply the Stoner model for itinerant ferromagnets, where the electrons of majority and minority spins are treated separately. Although this model completely neglects magnons, it reproduces the equilibrium magnetization of nickel for finite temperatures by using a realistic density of states and a dynamic exchange splitting [14].

*bmueller@physik.uni-kl.de

Within each electron system, the thermalization process after laser excitation occurs on a very short time scale in the order of 100 fs [30]. However, the equilibration between both electron systems takes longer and the temperatures of both electron types, denoted by $T_e^\uparrow$ and $T_e^\downarrow$, respectively, may differ for longer times. Moreover, the respective particle densities may change due to EY spin-flip processes and only their sum $n = n^\uparrow + n^\downarrow$ is constant. Therefore, the chemical potentials $\mu^\uparrow$ and $\mu^\downarrow$ have to be considered as further variables of $\vec{X}$ in Eq. (1). Further, in the frame of an effective Stoner model [14,24], the densities of states $D^\uparrow(E)$ and $D^\downarrow(E)$ of up and down electrons, respectively, are shifted by an exchange splitting Δ. This exchange splitting is not constant, but is directly coupled with the magnetization m through the effective Coulomb interaction U [24]. In Ref. [14] it was shown that the instantaneous feedback of the transient magnetization on the exchange splitting

$$\Delta(t) = Um(t), \tag{2}$$

is essential for the quantitative description of demagnetization dynamics. The normalized magnetization $m(t)$ results from the transient particle density of each electron reservoir as

$$m(t) = (n^\uparrow(t) - n^\downarrow(t))/n. \tag{3}$$

The particle density of the electrons $n^\sigma(T_e^\sigma,\mu^\sigma,m) = \int f(E,T_e^\sigma,\mu^\sigma)D(E,m)\,dE$ and internal energy density $u_e^\sigma(T_e^\sigma,\mu^\sigma,m) = \int f(E,T_e^\sigma,\mu^\sigma)D(E,m)E\,dE$ with the spin $\sigma \in \{\uparrow,\downarrow\}$ are calculated by the zeroth and first moment of the current Fermi distribution $f(E,T_e^\sigma,\mu^\sigma)$. Thus, under the given conditions both particle density and internal energy density depend on the two intrinsic variables T_e^σ and μ^σ and on the magnetization which determines the energy shift of the exchange splitting Δ, see Eq. (2). The temporal derivatives of the energy density u_e^σ and the particle density n^σ include partial derivatives, e.g.,

$$\frac{du_e^\sigma}{dt} = c_T^\sigma \frac{\partial T_e^\sigma}{\partial t} + c_\mu^\sigma \frac{\partial \mu^\sigma}{\partial t} + c_m^\sigma \frac{\partial m}{\partial t}, \tag{4}$$

defining the capacity equivalents $c_x^\sigma \equiv \frac{\partial u_e^\sigma}{\partial x}$. Analogously, partial derivatives of the particle density are defined as $p_x^\sigma \equiv \frac{\partial n^\sigma}{\partial x}$. This allows us to mathematically separate the variables T_e^σ, μ^σ, and m.

To demonstrate the power of the μT model and to separate the time-dependent effects from transport effects [22], we restrict ourselves here to the temporal dependence of the decisive variables, which is capable of predicting and explaining important characteristics of the magnetization dynamics of thin ferromagnetic films. The temporal evolution of $T_e^\uparrow, T_e^\downarrow, T_\ell, \mu^\uparrow, \mu^\downarrow$, and m is expressed with an equation of type (1)

$$\begin{pmatrix} c_T^\uparrow & 0 & 0 & c_\mu^\uparrow & 0 & c_m^\uparrow \\ 0 & c_T^\downarrow & 0 & 0 & c_\mu^\downarrow & c_m^\downarrow \\ 0 & 0 & c_\ell & 0 & 0 & 0 \\ p_T^\uparrow & 0 & 0 & p_\mu^\uparrow & 0 & p_m^\uparrow \\ 0 & p_T^\downarrow & 0 & 0 & p_\mu^\downarrow & p_m^\downarrow \\ -p_T^\uparrow & p_T^\downarrow & 0 & -p_\mu^\uparrow & p_\mu^\downarrow & n^\uparrow + n^\downarrow \end{pmatrix} \frac{d}{dt} \begin{pmatrix} T_e^\uparrow \\ T_e^\downarrow \\ T_\ell \\ \mu^\uparrow \\ \mu^\downarrow \\ m \end{pmatrix} =$$

$$\begin{pmatrix} -\gamma - g^\uparrow & \gamma & g^\uparrow & 0 & 0 & 0 \\ \gamma & -\gamma - g^\downarrow & g^\downarrow & 0 & 0 & 0 \\ g^\uparrow & g^\downarrow & -g^\uparrow - g^\downarrow & 0 & 0 & 0 \\ 0 & 0 & 0 & -\nu & \nu & 0 \\ 0 & 0 & 0 & \nu & -\nu & 0 \\ 0 & 0 & 0 & 0 & 0 & 0 \end{pmatrix} \begin{pmatrix} T_e^\uparrow \\ T_e^\downarrow \\ T_\ell \\ \mu^\uparrow \\ \mu^\downarrow \\ m \end{pmatrix} + \begin{pmatrix} S^\uparrow(t) \\ S^\downarrow(t) \\ 0 \\ 0 \\ 0 \\ 0 \end{pmatrix}. \tag{5}$$

The first three equations determine the energy of spin-up and spin-down electrons as well as of the lattice, respectively. Equations four and five trace the densities of both electron systems. The last equation defines the transient magnetization, Eq. (3). In the spirit of the TTM [23], we introduce a respective equilibration term for the electron temperatures, $\pm\gamma(T_e^\uparrow - T_e^\downarrow)$, and chemical potentials $\pm\nu(\mu^\uparrow - \mu^\downarrow)$. This is in accordance with a first-order approximation of the collision integrals in Refs. [14,30]. A comparison to Ref. [14] reveals that the parameters γ and ν are directly proportional to the spin-flip matrix element $|\langle\uparrow|\downarrow\rangle|^2$, hence proportional to the spin-mixing parameter b^2. The laser excitation of each electron system is described by the source term $S^\sigma(t)$. To reduce the number of parameters, we assume that both electron reservoirs absorb the same energy during irradiation $S^\uparrow = S^\downarrow$. However, due to the different densities, the electron temperatures and chemical potentials of up and down electrons may differ after excitation. To conserve the total energy with a dynamic exchange splitting, the correlation energy [24] $u_{\mathrm{Corr}}(t) = -Un^\uparrow(t)n^\downarrow(t)/n$ has to be taken into account in Eq. (5), but this is not shown for illustrative purposes.

The formulation of the μTM is not limited to Elliott-Yafet spin-flip mechanisms of electrons and phonons. Other processes, for instance electron-defect spin-flips, could be treated by our approach. Regardless of the underlying spin-flip channel, the μTM assumes that the total angular momentum of the system including both lattice and electrons with their dynamic band structure, is conserved. A further point of the μTM is that the exchange splitting vanishes for temperatures above Curie temperature T_C in equilibrium. However, it has been shown experimentally [31] that even above T_C a finite exchange splitting exists. These magnetic short-range order effects are difficult to describe theoretically [32] and they are not covered by our approach. The result of the μTM should be interpreted in terms of a long-range order magnetization.

III. RESULTS

We solve the μTM for a thin nickel film with the density of states from Ref. [33]. The thickness of the sample $z = 15$ nm is in the order of the penetration depth and we assume a homogeneously heated film [21]. In this case, the experimentally applied laser fluence after reflection $(1-R)F = z\int(S^\uparrow + S^\downarrow)dt$ can be related to the laser source term S^σ of the μTM. Applying an effective Coulomb interaction $U = 5.04$ eV to the Stoner model, the experimental equilibrium magnetization curve [34] is well reproduced [14]. Here, the Stoner model underestimates the magnetic moment $\mu_{\mathrm{mag}} = 0.51\mu_B$, in comparison to the literature value $\mu_{\mathrm{mag}} = 0.62\mu_B$ [35]. The deviations between theory and experiment result from neglecting magnons in the ferromagnetic description. These

TABLE I. Entries of the matrix C, determined for nickel at room temperature, in dependence on the spin $\sigma \in \{\uparrow,\downarrow\}$. Note that these parameters vary strongly during the calculation. The parameter p_m^σ vanishes for all times.

	$\uparrow$	$\downarrow$
c_T^σ[J/m^{3}K]	-1.44×10^7	1.01×10^7
c_μ^σ[1/m^3]	1.45×10^{30}	2.67×10^{30}
c_m^σ[J/m^3]	3.51×10^{11}	-3.83×10^{11}
p_T^σ[1/m^{3}K]	-1.21×10^{25}	8.28×10^{24}
p_μ^σ[1/m^{3}J]	1.21×10^{48}	2.29×10^{48}

low-energy excitations are sketched by a lower magnetic moment which in turn leads to a lower exchange splitting.

The lattice heat capacity is taken as $c_\ell = 3.776 \times 10^6$ J/Km^3 [35]. For simplicity, we introduce the same electron-lattice coupling $g^\sigma = g/2 = 1 \times 10^{18}$ W/Km^3 from Ref. [30] for both electron systems. The coupling parameters between chemical potentials $\nu = 5.80 \times 10^{60}$ 1/Jsm^3 and the inner-electronic temperature coupling $\gamma = 163.8 \times g^\sigma$ are newly introduced in this work. They are determined through a fit of the transient magnetization curve obtained by the μTM to experimental data of Ref. [21]. The entries of matrix C change strongly during the calculation interval. Therefore, they are determined dynamically for each time step. Table I lists the parameters for nickel at room temperature.

The Gaussian pump pulse of 50 fs (FWHM) at a wavelength of 800 nm was chosen according to the experiment [21]. With the reflectivity of $R = 0.55$, the μTM reproduces the magnetization curve for different fluences. A comparison between the experiment and the μT model is depicted in the upper panel of Fig. 1.

Figure 1 shows from top to bottom the dynamics of the magnetization, of the chemical potentials $\mu^\uparrow$, and $\mu^\downarrow$ and of the temperatures $T_e^\uparrow$, $T_e^\downarrow$, and T_ℓ. Two different fluences were applied for the calculations $F_0 = 2.5$mJ/cm^2 (blue curves) and $2 \times F_0$ (red curves). The minima of the magnetization curves are marked with vertical lines through all three panels of Fig. 1. The chemical potentials (central panel) of the majority and minority electrons differ strongly during irradiation, equal each other for an instant crossover, and equilibrate on later time scales. The electron temperatures (lower panel) both grow fast during irradiation, however, majority and minority temperatures differ due to the different heat capacities. After excitation, both electron temperatures equilibrate with each other and later also with the lattice temperature.

Inverting the capacity matrix C in Eq. (5) leads to a direct formulation for the temporal derivatives of $T_e^\uparrow, T_e^\downarrow, T_\ell, \mu^\uparrow, \mu^\downarrow$, and m. In particular, the change of magnetization is given by

$$\frac{dm}{dt} = -\frac{2\nu}{n}(\mu^\uparrow - \mu^\downarrow), \tag{6}$$

where the time dependence occurs only in the difference of the chemical potentials. Thus, in the μTM the equilibration of the chemical potentials of majority and minority electrons is the driving force of the magnetization dynamics, as proposed in Ref. [13].

IV. MAGNETIZATION CURVE CHARACTERISTICS

Five characteristic points appear in the magnetization dynamics. They are indicated in the magnetization curve for the lower excitation in Fig. 1. Their origins are explained with the μT model in the following.

(i) We analyze the magnetization dynamics directly at the time when the laser hits the sample. In this case, the μTM predicts a vanishing first derivative dm/dt for the initial time step, when the chemical potentials are still in equilibrium $\mu^\uparrow = \mu^\downarrow$, see Eq. (6). The feedback effect, induced by a dynamic exchange splitting only occurs at later times, when the chemical potentials are driven out of equilibrium. The μTM explicitly accounts for the feedback effect and its influence can be illustrated by calculating the second derivative of Eq. (5) during a constant laser excitation

$$\frac{d^2m}{dt^2} = -\left(\frac{p_T^\uparrow}{c_\mu^\uparrow p_T^\uparrow - c_T^\uparrow p_\mu^\uparrow} - \frac{p_T^\downarrow}{c_\mu^\downarrow p_T^\downarrow - c_T^\downarrow p_\mu^\downarrow}\right)\frac{\nu S}{n},$$

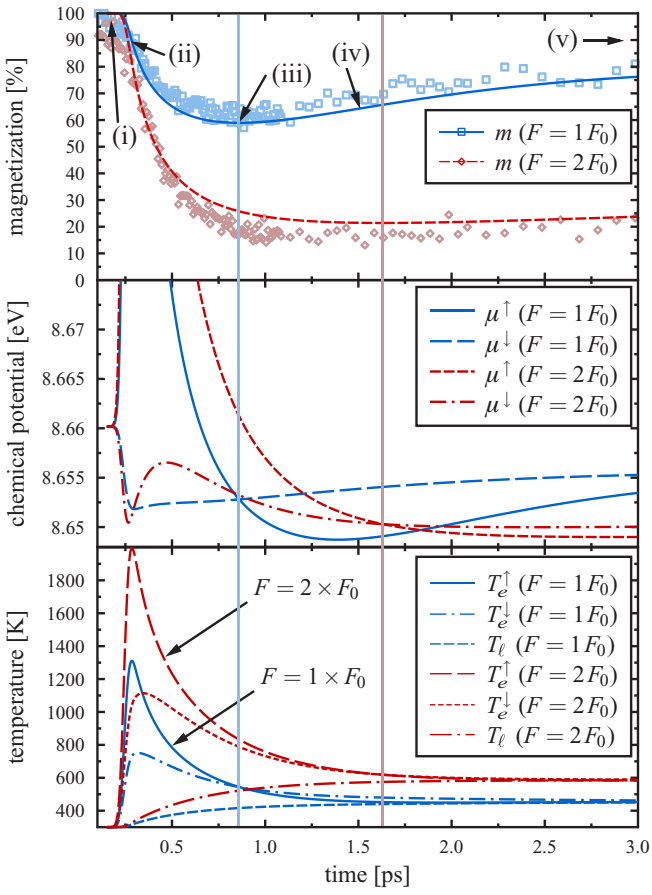

FIG. 1. (Color online) Typical results of the μT model, transient magnetization (upper panel), chemical potentials (central panel), and temperatures (lower panel). The blue curves correspond to a low fluence $F_0 = 2.5$mJ/cm^2, whereas the red curves are calculated after excitation with twice of that fluence, $2 \times F_0$. In the upper panel, experimental results [21] are shown for comparison. The vertical lines indicate the respective time where the magnetization dynamics suffer a minimum. Characteristic points (i) to (v), as marked for the blue solid demagnetization curve, are analyzed in the text.

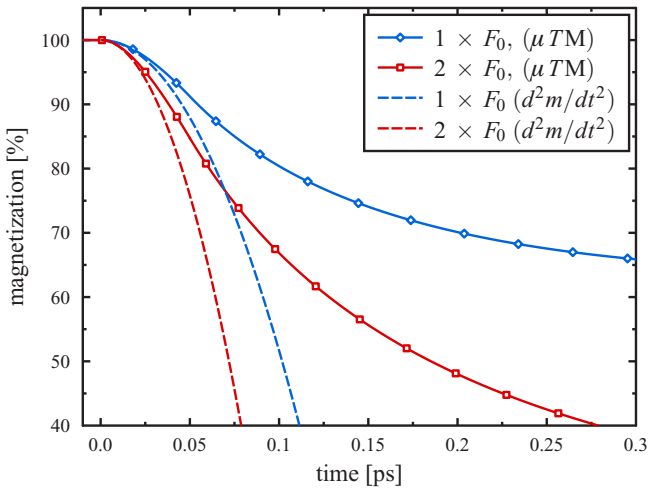

FIG. 2. (Color online) Magnetization dynamics for a rectangular laser pulse with the duration of 50 fs. Two fluences $F = 1 \times F_0$ and $F = 2 \times F_0$ are applied. For a direct comparison, the approximation $m(t) \approx m_0 + \frac{1}{2}\frac{d^2m}{dt^2}t^2$ is depicted in the diagram.

assuming G and C as constant over the considered time interval. Initially, $d^2m/dt^2 \propto S(t=0)$ holds for very short times and the transient magnetization is determined mainly by $m(t) \approx m_0 + \frac{1}{2}\frac{d^2m}{dt^2}t^2$. A direct comparison between this approximated form and the complete μTM is shown in Fig. 2. In this calculation, a rectangular pulse shape is applied and the fluences are the same as in Fig. 1. A parabolic decrease is observed even for the rectangular laser pulse and the approximation gives reasonable estimates for the first 50 fs.

Recent *ab initio* calculations determine the initial change of magnetization, $dm/dt|_{t=0}$, utilizing EY spin-flip processes [5,6,11]. They predict a much smaller demagnetization than it was observed in the experiment. Since the feedback effect [14] has not been taken into account, these calculations do not contradict the EY picture.

(ii) During laser excitation, the magnetization decreases rapidly, reaching the maximum change at the inflection point of the magnetization curve. Equation (6) proposes that also the nonequilibrium of chemical potentials is at its maximum, which is supported by Fig. 1. The difference in chemical potentials is explained by inverting the matrix C of the μTM:

$$\frac{d\mu^\sigma}{dt} = \frac{g^\sigma\left(T_\ell - T_e^\sigma\right) + \gamma\left(T_e^{\bar\sigma} - T_e^\sigma\right) + \nu(\mu^\sigma - \mu^{\bar\sigma})\xi + S^\sigma}{c_\mu^\sigma - c_T^\sigma p_\mu^\sigma / p_T^\sigma}, \tag{7}$$

with the abbreviation $\xi = (c_T^\sigma n + 2c_m^\sigma p_T^\sigma)/(np_T^\sigma)$. During laser excitation, the last summand of the numerator in Eq. (7) dominates, i.e., $\frac{d\mu^\sigma}{dt} \approx S^\sigma/(c_\mu^\sigma - c_T^\sigma p_\mu^\sigma/p_T^\sigma)$. Even for the same energy absorption $S^\uparrow = S^\downarrow$, a nonequilibrium in chemical potentials is established. This is due to the different response of up and down electrons to heating: The shifted density of states causes different entries of the matrix C for both spin types, as listed in Table I. Applying ultrashort laser excitation, also nonequilibrium effects may come into play [30,36]. However, it has been shown by a kinetic approach that for the given material and excitation parameters the nonequilibrium of the electrons plays a minor role in ultrafast magnetization dynamics [14]. An analysis based on thermal properties is therefore justified.

(iii) At the minimum of magnetization a transient equilibrium between the electron subsystems is observed. Here, the chemical potentials $\mu^\uparrow = \mu^\downarrow$ [as expected from Eq. (6)] and also the temperatures $T_e^\uparrow = T_e^\downarrow$ are equilibrated, both confirmed by Fig. 1. However, the lattice is still not in equilibrium with the electron system. In this transient equilibrium state, the μTM shows that the parabola approximation of the minimum,

$$\frac{d^2m}{dt^2} = \frac{2g\nu}{n}\left(\frac{p_T^\uparrow}{c_\mu^\uparrow p_T^\uparrow - c_T^\uparrow p_\mu^\uparrow} - \frac{p_T^\downarrow}{c_\mu^\downarrow p_T^\downarrow - c_T^\downarrow p_\mu^\downarrow}\right)(T_e - T_\ell),$$

is mainly determined by the temperature difference between the electrons and the lattice.

(iv) After the transient equilibrium state of the electron subsystems, the chemical potentials are driven out of equilibrium again. This is due to the relaxation with the lattice. At the maximum difference between both chemical potentials, the second inflection point in the magnetization curve occurs.

(v) For larger times, the chemical potentials and temperatures of the electrons and the lattice equilibrate, see Fig. 1, and the magnetization reaches its equilibrium value $m(T_e)$.

V. MAGNETIC PHASE DIAGRAM

The strength of the μTM is the possibility of analytical predictions about many relevant physical processes in ultrafast magnetization dynamics. In particular, we observe in Fig. 1 a so-called *critical slowing down* of magnetization dynamics [28,37] for the high laser fluence. The reason is explained in Fig. 3, which depicts the phase diagram of m and T_e:

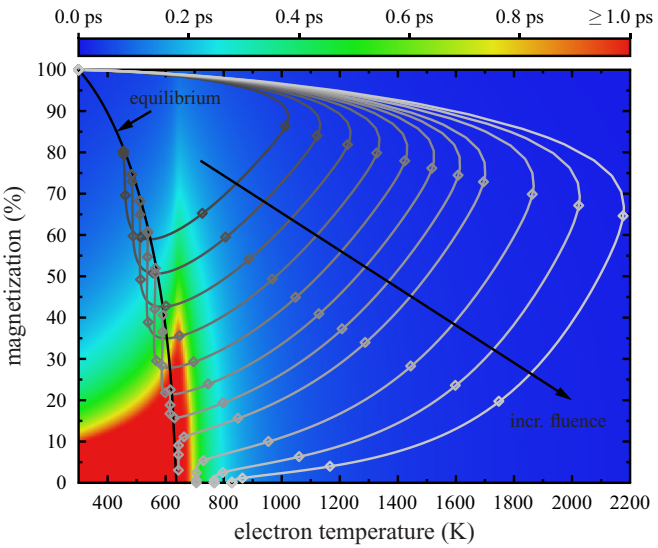

FIG. 3. (Color online) Phase diagram of ultrafast magnetization dynamics. The black curve is the equilibrium magnetization cuve $m(T)$. The gray curves result from the μT model for the fluences $F/F_0 = 1.0, 1.2, \ldots, 2.4, 2.8, 3.2, 3.6$ with $F_0 = 2.5\,\mathrm{mJ/cm^2}$. The symbols mark several times at $t = 0, 0.3, 0.5, 1, 2, 5, 10, 25$ ps. The background color labels the relaxation time towards the equilibrium magnetization.

For long excitations, in the order of nanoseconds, we expect that the magnetization follows the equilibrium magnetization $m(T_e)$, which is indicated as a black curve. However, the ultrashort laser pulse drives the system out of equilibrium and the magnetization becomes a function of $T_e^{\uparrow}, T_e^{\downarrow}, \mu^{\uparrow}$, and $\mu^{\downarrow}$. In particular, in these nonequilibrium states, the chemical potentials differ strongly, which is reflected in the central panel of Fig. 1. The temperatures $T_e^{\uparrow}$ and $T_e^{\downarrow}$ are close to each other and are approximated by their mean value T_e for the following discussion. In Fig. 3, the parametric (m, T_e) curves of magnetization dynamics after different laser fluences are indicated by gray lines. All curves start at room temperature, top left of the diagram. Further symbols up to 25 ps show the dynamical behavior on the parametric curves. The laser drives the system to high electron temperatures, however, due to the nonequilibrium situation, the magnetization is still finite even for $T_e > T_C$. The first crossover with the equilibrium magnetization curve, observed for fluences up to $2.2 \times F_0$, corresponds to the *transient equilibrium state* (iii) and coincides with the minimum of the respective magnetization curve.

Importantly, the time to reach the final state on the equilibrium magnetization curve $m(T_e)$ differs for different fluences. For each pair (m, T_e) both chemical potentials $\mu^{\uparrow}, \mu^{\downarrow}$ can be determined by simultaneously solving Eq. (3) and the equation of particle conservation, $n = \text{const}$. We can estimate the time τ_{eq} to reach the equilibrium magnetization (black curve) for each point of m and T_e in the phase diagram by a relaxation time approximation of Eq. (6),

$$\frac{m(T_e) - m(T_e, \mu^{\uparrow}, \mu^{\downarrow})}{\tau_{\text{eq}}} = -\frac{2\nu}{n}(\mu^{\uparrow} - \mu^{\downarrow}). \tag{8}$$

The relaxation time to equilibrium, τ_{eq}, is depicted in the background color code of Fig. 3. Under strong nonequilibrium conditions, especially at high temperatures, this relaxation occurs very fast: The large difference in chemical potentials rapidly drives the magnetization to its equilibrium value. However, around the Curie temperature at 631 K [35], the chemical potentials are nearly equal and the equilibration time according to Eq. (8) reaches rather high values up to nanoseconds, thus, the magnetization dynamics is extremely decelerated. The fluences $F/F_0 \approx 2.0$–2.4 drive the system into this critical region, appearing red in Fig. 3. For low and very high laser fluences this region is circumvented. Thus, the μTM directly illustrates the origin of a critical slowing down and explains why experiments show a maximum in demagnetization time [12], by utilizing basic thermodynamical concepts.

VI. CONCLUSION

In conclusion, we derived the μT model for itinerant ferromagnets. The description traces the dynamics of spin-resolved electron temperatures *and* chemical potentials simultaneously, combined with the coupling to the lattice. The demagnetization process can be described based on a few fundamental physical concepts, like dynamic exchange splitting and the relaxation towards thermodynamic equilibrium. Our method identifies the minimum of the magnetization as a transient equilibrium state of the electron systems. We explain the experimentally observed slowing down of the magnetization dynamics by a critical region in the magnetic phase diagram, Fig. 3. For certain fluences, the system is driven into this region and the time to reach the equilibrium magnetization increases considerably.

ACKNOWLEDGMENTS

We thank Martin Aeschlimann, Hans Christian Schneider, Linda Thesing, and Anika Rämer for fruitful discussions. Financial support of the Deutsche Forschungsgemeinschaft through the Heisenberg Project No. RE 1141/15 "Ultrafast Dynamics of Laser-excited Solids" is gratefully acknowledged.

[1] T. W. McDaniel, J. Phys.: Condens. Matter **17**, R315 (2005).
[2] E. Beaurepaire, J.-C. Merle, A. Daunois, and J.-Y. Bigot, Phys. Rev. Lett. **76**, 4250 (1996).
[3] A. J. Schellekens, W. Verhoeven, T. N. Vader, and B. Koopmans, Appl. Phys. Lett. **102**, 252408 (2013).
[4] A. J. Schellekens and B. Koopmans, Phys. Rev. Lett. **110**, 217204 (2013).
[5] C. Illg, M. Haag, and M. Fähnle, Phys. Rev. B **88**, 214404 (2013).
[6] K. Carva, M. Battiato, and P. M. Oppeneer, Phys. Rev. Lett. **107**, 207201 (2011).
[7] M. Battiato, K. Carva, and P. M. Oppeneer, Phys. Rev. Lett. **105**, 027203 (2010).
[8] A. Eschenlohr, M. Battiato, P. Maldonado, N. Pontius, T. Kachel, K. Holldack, R. Mitzner, A. Föhlisch, P. M. Oppeneer, and C. Stamm, Nat. Mater. **12**, 332 (2013).
[9] E. Turgut, C. La-o-vorakiat, J. M. Shaw, P. Grychtol, H. T. Nembach, D. Rudolf, R. Adam, M. Aeschlimann, C. M. Schneider, T. J. Silva, M. M. Murnane, H. C. Kapteyn, and S. Mathias, Phys. Rev. Lett. **110**, 197201 (2013).
[10] S. Kaltenborn, Y.-H. Zhu, and H. C. Schneider, Phys. Rev. B **85**, 235101 (2012).
[11] S. Essert and H. C. Schneider, Phys. Rev. B **84**, 224405 (2011).
[12] B. Koopmans, G. Malinowski, F. Dalla Longa, D. Steiauf, M. Fähnle, T. Roth, M. Cinchetti, and M. Aeschlimann, Nat. Mater. **9**, 259 (2010).
[13] B. Y. Mueller, T. Roth, M. Cinchetti, M. Aeschlimann, and B. Rethfeld, New J. Phys. **13**, 123010 (2011).
[14] B. Y. Mueller, A. Baral, S. Vollmar, M. Cinchetti, M. Aeschlimann, H. C. Schneider, and B. Rethfeld, Phys. Rev. Lett. **111**, 167204 (2013).
[15] M. Krauss, T. Roth, S. Alebrand, D. Steil, M. Cinchetti, M. Aeschlimann, and H. C. Schneider, Phys. Rev. B **80**, 180407(R) (2009).
[16] D. Steil, S. Alebrand, T. Roth, M. Krauß, T. Kubota, M. Oogane, Y. Ando, H. C. Schneider, M. Aeschlimann, and M. Cinchetti, Phys. Rev. Lett. **105**, 217202 (2010).
[17] B. Koopmans, J. J. M. Ruigrok, F. Dalla Longa, and W. J. M. de Jonge, Phys. Rev. Lett. **95**, 267207 (2005).
[18] M. Fähnle, J. Seib, and C. Illg, Phys. Rev. B **82**, 144405 (2010).

[19] J. Walowski, G. Müller, M. Djordjevic, M. Münzenberg, M. Kläui, C. A. F. Vaz, and J. A. C. Bland, Phys. Rev. Lett. **101**, 237401 (2008).
[20] E. Carpene, E. Mancini, C. Dallera, M. Brenna, E. Puppin, and S. De Silvestri, Phys. Rev. B **78**, 174422 (2008).
[21] T. Roth, A. J. Schellekens, S. Alebrand, O. Schmitt, D. Steil, B. Koopmans, M. Cinchetti, and M. Aeschlimann, Phys. Rev. X **2**, 021006 (2012).
[22] A. Rämer, O. Osmani, and B. Rethfeld, J. Appl. Phys. **116**, 053508 (2014).
[23] S. I. Anisimov, B. L. Kapeliovich, and T. L. Perel'man, Zh. Eksp. Teor. Fiz. **66**, 776 (1974) [Sov. Phys. JETP **39**, 375 (1974)].
[24] W. Nolting and A. Ramakanth, *Quantum Theory of Magnetism*, 1st ed. (Springer, Berlin, 2009).
[25] A. Manchon, Q. Li, L. Xu, and S. Zhang, Phys. Rev. B **85**, 064408 (2012).
[26] P. Bruno, Phys. Rev. Lett. **90**, 087205 (2003).
[27] M. Haag, C. Illg, and M. Fähnle, Phys. Rev. B **90**, 014417 (2014).
[28] M. G. Münzenberg, Nat. Mater. **9**, 184 (2010).
[29] H.-S. Rhie, H. A. Dürr, and W. Eberhardt, Phys. Rev. Lett. **90**, 247201 (2003).
[30] B. Y. Mueller and B. Rethfeld, Phys. Rev. B **87**, 035139 (2013).
[31] D. E. Eastman, F. J. Himpsel, and J. A. Knapp, Phys. Rev. Lett. **40**, 1514 (1978).
[32] V. Antropov, Phys. Rev. B **72**, 140406 (2005).
[33] Z. Lin, L. V. Zhigilei, and V. Celli, Phys. Rev. B **77**, 075133 (2008).
[34] F. Tyler, Philosophical Magazine Series 7 **11**, 596 (1931).
[35] D. R. Lide, G. Baysinger, L. I. Berger, R. N. Goldberg, H. V. Kehiaian, K. Kuchitsu, G. Rosenblatt, D. L. Roth, and D. Zwillinger, *CRC Handbook of Chemistry and Physics*, 86th ed., (CRC, Boca Raton, FL, 2005).
[36] K. Carva, D. Legut, and P. M. Oppeneer, Europhys. Lett. **86**, 57002 (2009).
[37] O. Chubykalo-Fesenko, U. Nowak, R. W. Chantrell, and D. Garanin, Phys. Rev. B **74**, 094436 (2006).